RSC Advances

PAPER

Cite this: *RSC Adv.*, 2023, **13**, 34947

Reliable lateral Zn deposition along (002) plane by oxidized PAN separator for zinc-ion batteries†

Lei Luo,[a] Zhaorui Wen,[a] Guo Hong *[b] and Shi Chen *[a]

Aqueous zinc ion batteries (AZIBs) are the promising candidate for energy storage where safety and low cost are the major concerns. However, the uneven and random electrodeposition of Zn has become a serious impediment to the deep recharging of AZIBs. Conventional modifications on zinc substrate can promote homogenous zinc deposition initially, but not sustainably. Here, an oxidized polyacrylonitrile (OPAN) membrane with a conjugated planar structure is proposed as a zinc ion battery separator. This separator can continuously regulate the growth of Zn with (002) texture to inhibit dendrites. In addition, the separator has a fast Zn^{2+} ion transfer, which can spontaneously repel SO_4^{2-} and relieve side reactions. As a result, the Zn-symmetric batteries show cycle lifetime of more than 1300 hours at 1 mA cm^{-2} and 1 mA h cm^{-2}, and kept stable for more than 160 hours even at 65% high discharge of depth (DOD). The MnO_2//Zn full celled assembled with an OPAN separator had very little decay for 5000 cycles at 2 A g^{-1}. This work provides a new method for realizing the continuous and uniform deposition of Zn metals, which also provides a new route for batteries with metallic anodes.

Received 31st July 2023
Accepted 27th October 2023

DOI: 10.1039/d3ra05177c

rsc.li/rsc-advances

1 Introduction

In recent years, aqueous zinc ion batteries (AZIBs), including Zn–air batteries, Zn–manganese dioxide batteries and Zn–nickel batteries, have attracted much attention due to the high specific energy density and low cost of Zn metal.[1–4] In addition, aqueous electrolytes are safer and provide higher ionic conductivity (*i.e.*, faster charge and discharge rates) than their organic counterparts.[5] However, the dendrite growth and the corrosion of Zn metal anode in aqueous condition leads to low Coulomb efficiency and short battery life, which is one of the major hurdles in the development of AZIBs.

A lot of works is devoted to stabilize Zn anode by various modification methods.[6] Such modification includes introducing a coating layer on Zn anode by carbon or inorganic porous materials,[7–10] or constructing three-dimensional structure/skeleton to increase the space to accommodate Zn deposition and to suppress side reactions.[11–14] In addition, optimizing the molecular structure of electrolyte was also proposed to adjust the coordination of Zn ions,[15–17] provoking a dendrite-free Zn deposition process. Recently, (002) textured metal Zn anode are found effective in dendrite suppression and attracts wide attentions. The Zn (002) plane not only has greater corrosion resistance than the Zn (101) and Zn (100) planes, it also reduces the contact area between electrodes and electrolytes, which aids in the reduction of side reactions and the improvement of battery performance (Fig. 1).[18–20] Many methods such as acid etching,[21] lattice-matching substrate guided Zn deposition[8,22–24] and of Zn alloying[25] can be used to create (002) textured Zn anodes. However, when the depth of discharge is high or the cycle time is long, the (002) textured Zn may be destroyed by repeat deposition/striping, losing its suppression effect.[26] Therefore, to maintain a durable (002) textured Zn surface is critical to extend the cycle stability of Zn metal anodes.

It should be noted that most of previous researches on suppressing dendrite growth in Zn ions battery focused on the Zn metal anode while ignoring the role of the separator. As a material in direct contact with cathode and anode, separator has a strong influence on Zn deposition/striping too. At present, the most commonly used separator in the Zn battery is glass fiber (GF) filter paper.[27–30] However, due to the shortcomings of GF separator, such as large and uneven pores, low mechanical strength and fragility, Zn dendrites are particularly easy to grow freely, puncturing the separator and resulting in short circuit.[31–33] Therefore, a dual function separator which is capable to regulate Zn deposition along (002) plane and separates anode and cathode could provide a durable dendrite suppression effect AZIBs. Polyacrylonitrile (PAN) with good electrochemical stability, great thermal stability, and high tensile strength and tensile modulus, has been reported as a potential separator material for LIBs and AZIBs.[34,35] Due to the strong coordination between Zn^{2+} and the cyano groups (–CN),

[a]*Institute of Applied Physics and Materials Engineering, University of Macau, Avenida da Universidade, Taipa, Macau SAR, 999078 China. E-mail: shichen@um.edu.mo*
[b]*Department of Materials Science and Engineering, Center of Super-Diamond and Advanced Films, City University of Hong Kong, 83 Tat Chee Avenue, Kowloon, Hong Kong SAR 999077, China. E-mail: guohong@cityu.edu.hk*

† Electronic supplementary information (ESI) available. See DOI: https://doi.org/10.1039/d3ra05177c

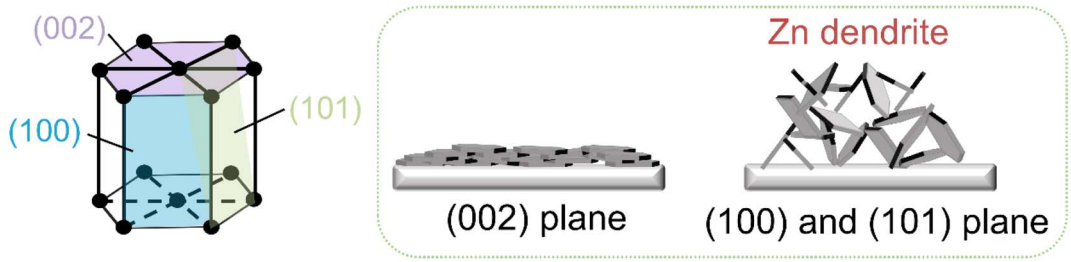

Fig. 1 Schematic illustration of Zn^{2+} deposition with (002) plane or (110) and (101) plane.

the PAN film shows effects in inhibition the uncontrolled deposition of Zn.[36,37] However, the metal Zn mainly grows along the (101) direction with PAN separator, limiting its long-term effect in dendrite suppression.

It is noticed that PAN can be converted into carbon fiber by oxidation and high temperature annealing. In the process of pre-oxidation at low temperature (200–300 °C), polyacrylonitrile mainly underwent cyclization reaction, dehydrogenation reaction, and oxidation reaction, transforming from thermoplastic linear aliphatic chain into non-plastic heat-resistant cross-linked carbon chain (conjugated planar structure) (Fig. S1†).[38,39] The conjugated structure, which is similar to the graphite structure, is also believed to have a very small lattice mismatch with Zn, thus inducing the formation of (002) textured Zn.

Therefore, we prepared nanofiber membrane from commercial PAN using electrostatic spinning and converted it into partially oxidized polyacrylonitrile (OPAN) separator. The OPAN separator has a small thickness (0.1 mm), good mechanical strength, and a high Zn^{2+} transference number (0.955). In particular, OPAN has a unique conjugated planar structure, which could regulate crystal growth direction of Zn ions, form Zn (002) crystal plane, and inhibit the growth of Zn dendrites. XRD showed that the dominant crystal plane of Zn anode after cycling with OPAN separator is transformed from the original (101) plane to (002) plane. SEM results also showed a flat Zn anode surface. Therefore, Zn anodes equipped with OPAN separator had lower polarizability (62 mV at 1 mA cm^{-2}) and longer cycling life (over 1300 h at 1 mA cm^{-2}). The Zn//Zn symmetric cells also had a long life of 160 h at high DOD (65%). The average Coulomb efficiency of Cu//Zn asymmetric cells is 99.1%. Consequently, the MnO_2–Zn cells using OPAN separator had high specific capacity (with capacities of 216, 194, 156, 139, and 113 mA h g^{-1} at 0.1, 0.2, 0.5, 1, and 2 A g^{-1}) and long-term durability of 5000 cycles at 2 A g^{-1} (90% capacity retention).

2 Experiment section

2.1 Preparation of OPAN membrane

PAN (molecular weight = 150 000, Aladdin Reagent Co., Ltd) was dissolved in *N*,*N*-dimethyl formamide (DMF, purity ≥ 99.8%, Aladdin Reagent Co., Ltd) to prepare a 10 wt% solution. The internal temperature of the electrospinning machine was room temperature, the humidity was 60%. The PAN solution was applied with 10–15 kV, with injection speed of 2.5 mL h^{-1}. The final product was dried at 80 °C for 12 h to obtain the PAN membrane. The PAN films were treated at 260 °C for 20 min to get the OPAN membrane. Cut it into 16 mm diameter discs to obtain OPAN separator for use.

2.2 Characterization

The X-ray diffraction XRD patterns were collected on Rigaku SmartLab (Japan) using Cu Kα radiation at a generator voltage of 40 kV. The scanning electron microscopy (SEM) images were collected at SEM, Zeiss SUPRA33-VP. The functional group changes of PAN before and after pre-oxidation were analyzed by Fourier transform infrared spectroscopy (FTIR, Bruker TENSOR II). The chemical transformations from PAN to OPAN were studied by X-ray photoelectron spectroscopy (XPS, Axis Ultra HAS) with an Al Kα X-ray source. The separators' mechanical strength was determined by WDS-6100 universal testing machine. The electrolyte absorption process of the separators was recorded by JC 2000D1 contact angle measuring instrument (Zhong Chen, Shanghai).

2.3 Electrochemical test

The Zn foil was cut into *Φ*12 mm discs and used directly as the anode. To make the cathode, a slurry of MnO_2 (Aladdin Reagent Co., Ltd), super P and sodium carboxymethylcellulose were mixed in a deionized water at a mass ratio of 7 : 2 : 1, then coated on titanium foil and dried overnight at 80 °C. The cathode material was also cut into *Φ*12 mm discs. The mass load of active substance on each slice was 1 mg cm^{-2}. Carbon nanotubes are used as the conductive agent in cathode of the full cell with a high mass loading of 5, 10, 15 mg cm^{-2}. The above components were assembled to CR2032 coin cells (room temperature in air) to evaluate the electrochemical performance. The fabrication of Zn//Zn symmetric cell, MnO_2//Zn cell, and Cu//Zn cell were prepared by 2 M $ZnSO_4$ electrolyte without any additive. The rate and cycling performance were tested on battery tester (NEWARE, Shenzhen, China). The cyclic voltammetry (CV) tests and electrochemical impedance spectroscopy (EIS) were performed at an electrochemistry workstation (CHI760, China).

3 Results and discussion

The PAN membrane was prepared by electrospinning followed by calendering to get a smooth surface (Fig. 2a). A separator

with a flat and uniform surface is preferred to produce a homogeneous and dense metal deposit layer. PAN was oxidized in air at 260 °C to form a conjugated planar structure. Fig. S1† illustrates the mechanism of the cyclization and oxidation of PAN in air.[38,39] PAN first underwent cyclization, that is, the oligomerization of adjacent cyanogen groups to the N-ring. In the subsequent thermal annealing process, the C=O groups generated in PAN oxidation underwent condensation dehydration reaction with nearby groups, resulting in a denser molecular network. The PAN membrane became dark because of the conjugation from the cyclization and oxidation reactions.

As shown in Fig. S2,† PAN membrane is a white film. After oxidation in the air, the PAN membrane became a brownish black OPAN membrane (Fig. 2b) but still maintained good flexibility (Fig. S3†). The thickness of OPAN membrane is 0.1 mm, much thinner than that of GF (0.23 mm), as depicted in Fig. S4,† which may reduce the length of the Zn ion diffusion pathway and increase the volumetric energy density of AZIBs. The SEM image (Fig. 2b) demonstrates that OPAN is interwoven with nanofibers with an average diameter of about 500 nm. The tensile curves of OPAN and GF are shown in Fig. 2c. The OPAN membrane shows much better mechanical strength than the GF membrane, with a maximum strength of 9.5 MPa, which is 9.5 times that of the GF membrane. Furthermore, the OPAN membrane has a larger stress elongation value (6.6%), indicating that it has exceptional inherent toughness. The water absorption process of the separators is shown in Fig. S5a,† both separators absorb the electrolyte quickly, but the initial contact Angle of OPAN (25.3°) is smaller than that of GF (39.3°). The electrolyte absorption of the separators is shown in Fig. S5b,† OPAN separator absorbed less electrolyte than GF, which increased the weight specific energy of the battery.[40] The results of the tests revealed good water wettability of both separators.

Ionic conductivity is an important battery characteristic. Although aqueous electrolytes have very strong ionic conductivity, separators would restrict their conductive capabilities. The EIS curves (Fig. S6a†) were used to calculate the apparent ionic conductivities of separators. As shown in Fig. S6b,† the apparent ionic conductivity of the OPAN membrane is 12.6 S m^{-1}, larger than that of glass fiber (7.5 S m^{-1}). The electrochemical characteristics of AZIBs were also considerably influenced by Zn^{2+} ion transfer value ($t_{Zn^{2+}}$).[41] The lower $t_{Zn^{2+}}$ value, the more Zn^{2+} ions are concentrated at the interface between the Zn metal anode and the electrolyte, increasing the challenge of Zn dendritic and parasitic side reactions. In our study, the $t_{Zn^{2+}}$ with OPAN and GF separators were estimated using the Zn//Zn cell by chronoamperometry (CA) method with a constant polarization potential of 25 mV (Fig. S7†). The calculation formula of $t_{Zn^{2+}}$ is showed in ESI.† According to Fig. 3a, the $t_{Zn^{2+}}$ value with the OPAN separator is 0.955, much higher than the GF separator (0.431), demonstrating that the OPAN separator could improve Zn^{2+} ion transport and alleviate the interface concentration gradient. Such effect could be explained by stronger electronegativity of the N atoms in the OPAN separator absorbs Zn^{2+}, repels the SO_4^{2-}, limiting anion migration and promoting cation transference.[42–44]

FT-IR spectra (Fig. 3b) presents the chemical transformations of PAN and OPAN membrane. The spectrum is labeled with a number of different bands corresponding to functional groups.[45–47] After the pre-oxidation of PAN membrane, the peak intensity of C≡N (2243 cm^{-1}) and CH_2 (1450 cm^{-1}) decreased significantly, while new peaks of C=C or C=N (1592 cm^{-1}) groups appeared. These peak intensity changes suggested triple bond opening and formation of the pyridine ring-containing conjugated planar structure during the oxidation. XPS results of the N 1s spectra in the Fig. 3a also confirmed the structural evolution of the PAN membrane interphase induced in annealing. The XPS N 1s spectrum of PAN only contains one N related bonding at 399.7 eV, which is

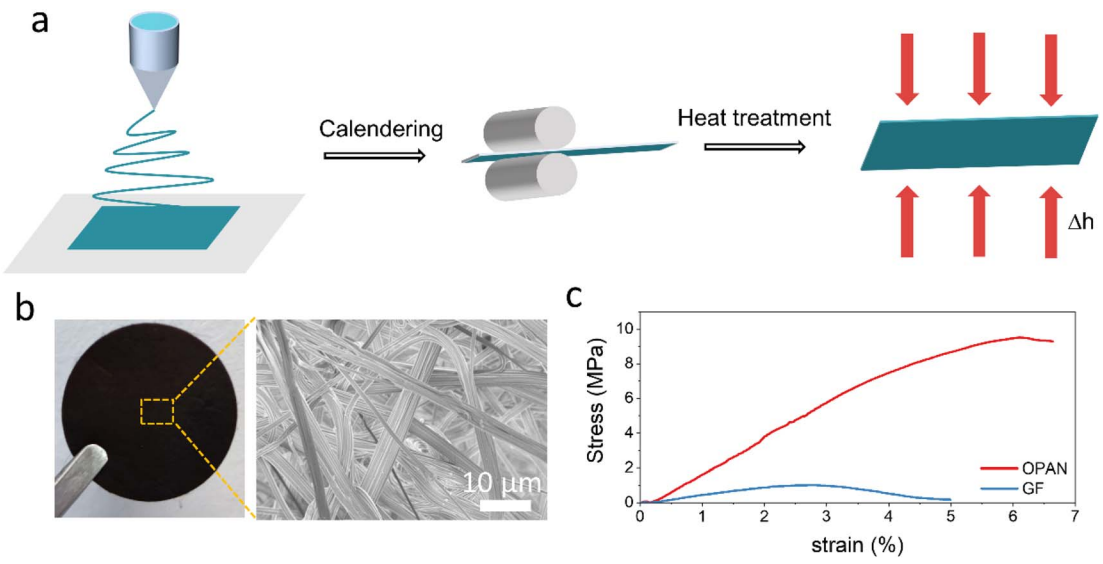

Fig. 2 (a) Diagram of OPAN membrane preparation; (b) optical photograph and SEM of OPAN membrane; (c) tensile strength of OPAN and GF membranes.

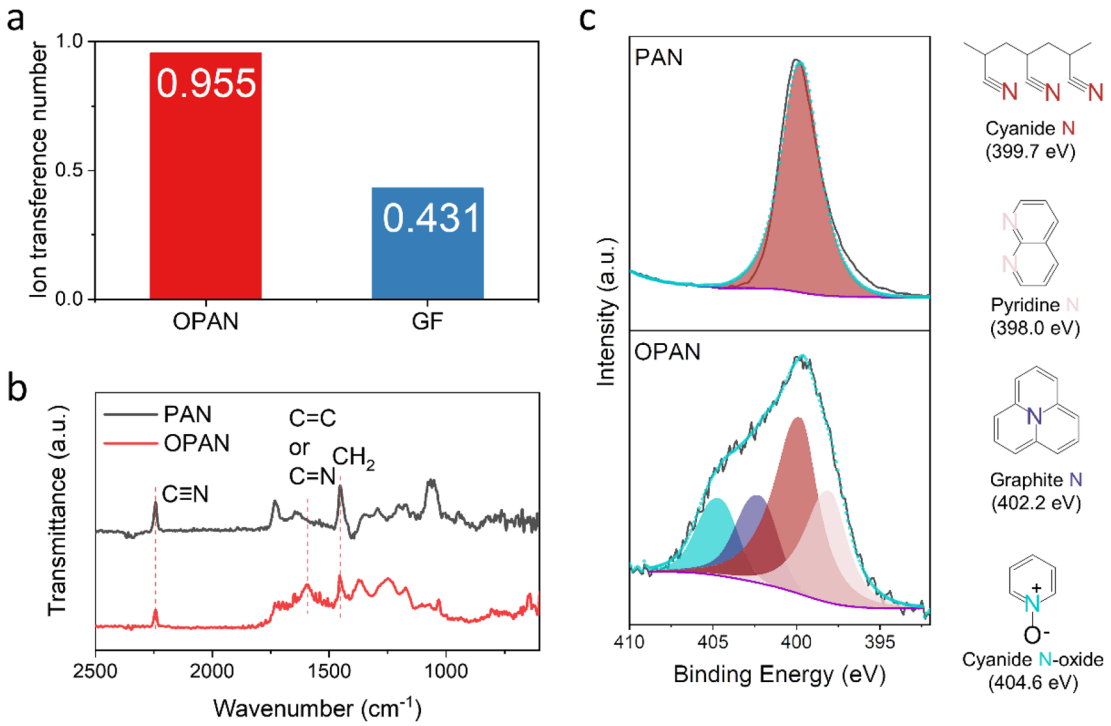

Fig. 3 (a) XPS N 1s spectrums of PAN and OPAN with their structures of all N species; (b) FT-IR spectra and (c) the ionic transference number of OPAN and GF membranes.

species from nitrile group (C≡N) (Fig. 3c). Meanwhile, the N 1s spectrum of OPAN shows a much-complicated peak envelope containing four different N bonds. Except the strongest components at 399.7 eV from C≡N bonds, new peaks from pyridine N (C–N=C, at 398.0 eV) and substituted graphite N (N coordination with three C atoms, at 402.2 eV) appear, which also proves the formation of the conjugated planar structure.[48,49] The fourth peak located at 404.6 eV is due to partial oxidation of PAN polymer forming a pyridine N-oxide bond (C=N^+–O^-).[50] The introduction of oxidation peak may explain its increased hydrophilicity.

The hexagonal lattice structure matches the electrodeposited Zn (002) planar lattice with the smallest lattice mismatch (7.4%).[51,52] Besides that, nitrogen-doped graphene can regulate the homogeneous nucleation and induce the deposition of Zn onto the (002) plane due to the high adsorption of Zn atoms to N-containing functional groups.[53] Therefore, the unique conjugated structure of OPAN can help to deposit Zn along the (002) plane. The Zn//Zn symmetrical cells using GF separator, PAN separator and OPAN separator were assembled for comparison. It was worth noting that in the cell assembly process, the OPAN separator can be tightly attached to the Zn anode surface under electrostatic interaction (Fig. S8†) and pressure. The symmetrical cells were cycled 5 times at the current density of 10 mA cm^{-2} and the areal capacity of 10 mA h cm^{-2} before dissembled for XRD measurement. In Fig. 4a, the pristine Zn foil contains various crystal planes while the (101) plane is the dominated one. The intensity ratio of $I_{(002)}/I_{(100)}$ in pristine Zn is 0.582 (Fig. 4c). In the cell with the GF separator, Zn deposition only slight increase of the $I_{(002)}/I_{(100)}$ ratio to 1.444. Similar observation can be found with the PAN separator, showing a $I_{(002)}/I_{(100)}$ ratio at 1.269 (Fig. S9†). In contrast, in the cell with the OPAN separator, the ratio of $I_{(002)}/I_{(100)}$ reaches 9.845, more than 10-fold higher than the pristine Zn foil. The increased diffraction peak ratio proved that the deposited Zn was mainly along the (002) plane. Such orientation change is also witnessed in SEM images. As shown in Fig. 4b, the surface of Zn anode with OPAN separator is flat with large hexagons microplates mainly stacked along the surface. However, the surface of Zn anode with GF separator (Fig. 4b) is much rougher, with a large number of small microplates mainly grown along the out of plane direction. Using PAN separators, Zn foil and PAN separator are difficult to peel off, and Zn is present in flake and granular shape, mixing with PAN fibers as shown in the insert of Fig. S9.† These results confirmed that the OPAN separator prepared by annealing process can promote the deposition of Zn along the (002) plane at the horizontal direction and significantly inhibits Zn dendrites formation.

Electrochemical hydrogen evolution can cause local concentration polarization of Zn^{2+} ions and surface side reactions of Zn anodes, resulting in severe Zn dendrites, which significantly reduce lifetime of ZIBs.[54,55] In general, the larger the hydrogen evolution overpotential, the greater the polarization, the more hydrogen evolution reaction can be alleviated.[56,57] Fig. 4d shows the results of linear scanning voltammetry (LSV). The hydrogen evolution potential of Zn anode using OPAN separator is 17 mV lower than that using GF separator, indicating lesser hydrogen evolution with OPAN separator. The

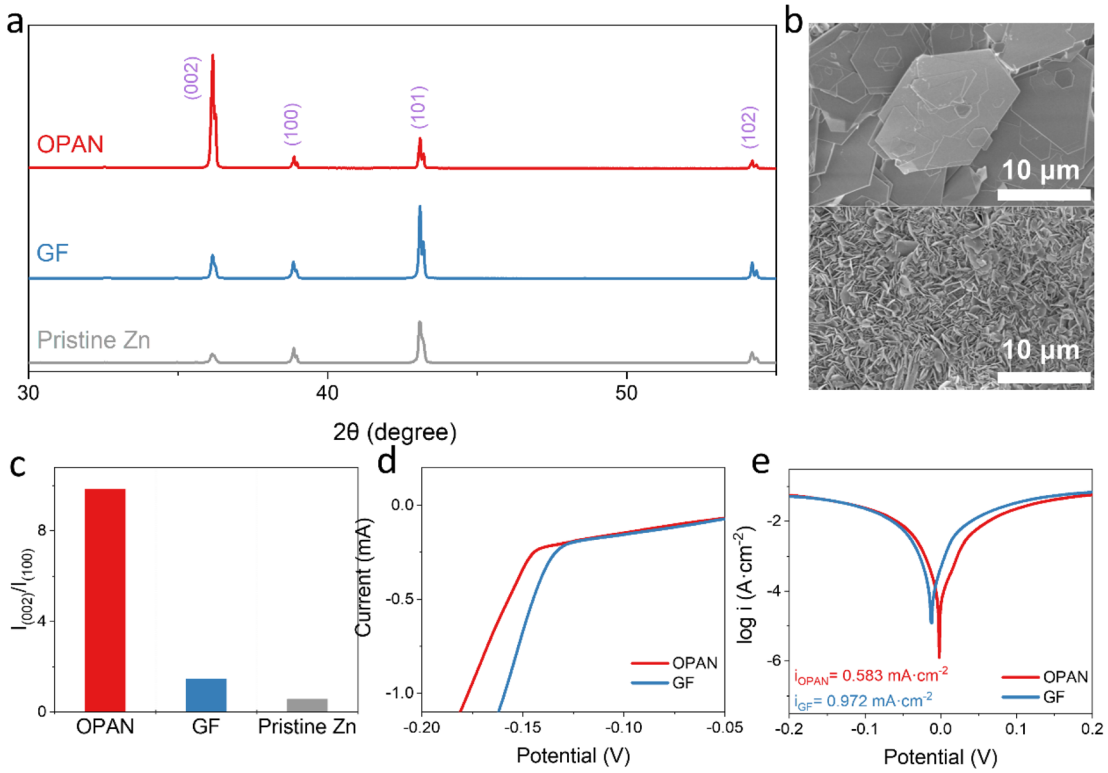

Fig. 4 (a) *Ex situ* XRD patterns of Zn anode using OPAN and GF separator after cycling; (b) SEM images of Zn anode using OPAN (upper) and GF separator (lower) after cycling; (c) the intensity ratio of (002) plane to (100) plane of Zn anode using OPAN and GF separator; (d) LSV curves at 1 mV s^{-1} of the Zn anode using OPAN and GF separator; (e) Tafel curves of Zn anode using OPAN and GF separator.

hydrogen evolution reaction can also be evaluated from the corrosion potential and corrosion current of the materials.[9,58] Compared with using GF separator, the Zn corrosion current density using OPAN separator decreased from 0.972 mA cm^{-2} to 0.583 mA cm^{-2}, and the corrosion potential increased from −13 mV to −2 mV, showing that Zn corrosion is significantly reduced using OPAN separator. In addition, if the hydrogen evolution reaction occurs, the concentration of OH^- ions in the electrolyte will increase, causing precipitation of side products like basic zinc sulfate, which is an inert layer and will hinder the transport of Zn ions. Compared with using GF separator, the XRD pattern of Zn using OPAN separator cycling (Fig. S10†) showed that no peak existed at $2\theta = 8°$ (corresponding to $Zn_4SO_4(OH)_6 \cdot xH_2O$ byproducts),[59] indicating that the side reaction could be reduced by using OPAN separator. In the electrochemical mechanism shown in Fig. 5a, the OPAN separator are in direct contact with Zn anode. The fibers of OPAN in contact or with very close proximity to the Zn anode could promote Zn deposition along (002) plane. For GF separators, no such regulation effect can be found. The Zn could grow randomly with no (002) preference.

In order to further evaluate the stability of Zn anode using different separator, the charge–discharge areal capacity was set to 1 mA h cm^{-2}, and the charge–discharge performance of Zn//Zn symmetrical cell was tested under different current densities. When the current density was 1 mA cm^{-2}, the voltage polarization (62 mV) of the cell using OPAN separator was lower than that using GF separator (93 mV) (Fig. S11a†), which is probably due to the high Zn^{2+} ion transference number of OPAN during Zn deposition, reducing Zn^{2+} ion gradient. The symmetrical cell with GF separator can only work stably for 40 h in continuous cycles (Fig. 5b). After that, a sudden irreversible decline of its voltage is detected, indicating that the cell is short-circuited, which causes it to fail. The symmetrical cell with PAN separator also only maintained 31 hours (Fig. S12a†), which is comparable to the GF separator. In contrast, the symmetrical cell using the OPAN separator shows a much longer cycle life (~1300 h) (Fig. 5b), which presents one of the advanced performances compared to other separators (Table S1†). When under a larger current density of 10 mA cm^{-2} (Fig. 5c and S12b†), the symmetrical cell assembled by the OPAN separator can still maintain a stable cycle for 726 hours, 3630 cycles, while the GF separator only can work for 5 hours and PAN separator work 10 hours. At such condition, the polarization voltages of the cells were significantly increased due to limited ion diffusion kinetics. However, the polarization voltage using OPAN separator (123 mV) is still smaller than using GF separator (146 mV) (Fig. S11b†). This observation confirms the higher Zn^{2+} ion transference number in OPAN separator. Furthermore, when the cell under high current density (10 mA cm^{-2}) and large areal capacity (5 mA h cm^{-2}) it could still cycle for 200 h with OPAN separator, which is 27 times longer than the cell using GF separator (Fig. S13†) and 33 times longer than the cell using PAN separator (Fig. S12c†). What's more, the current of the cell

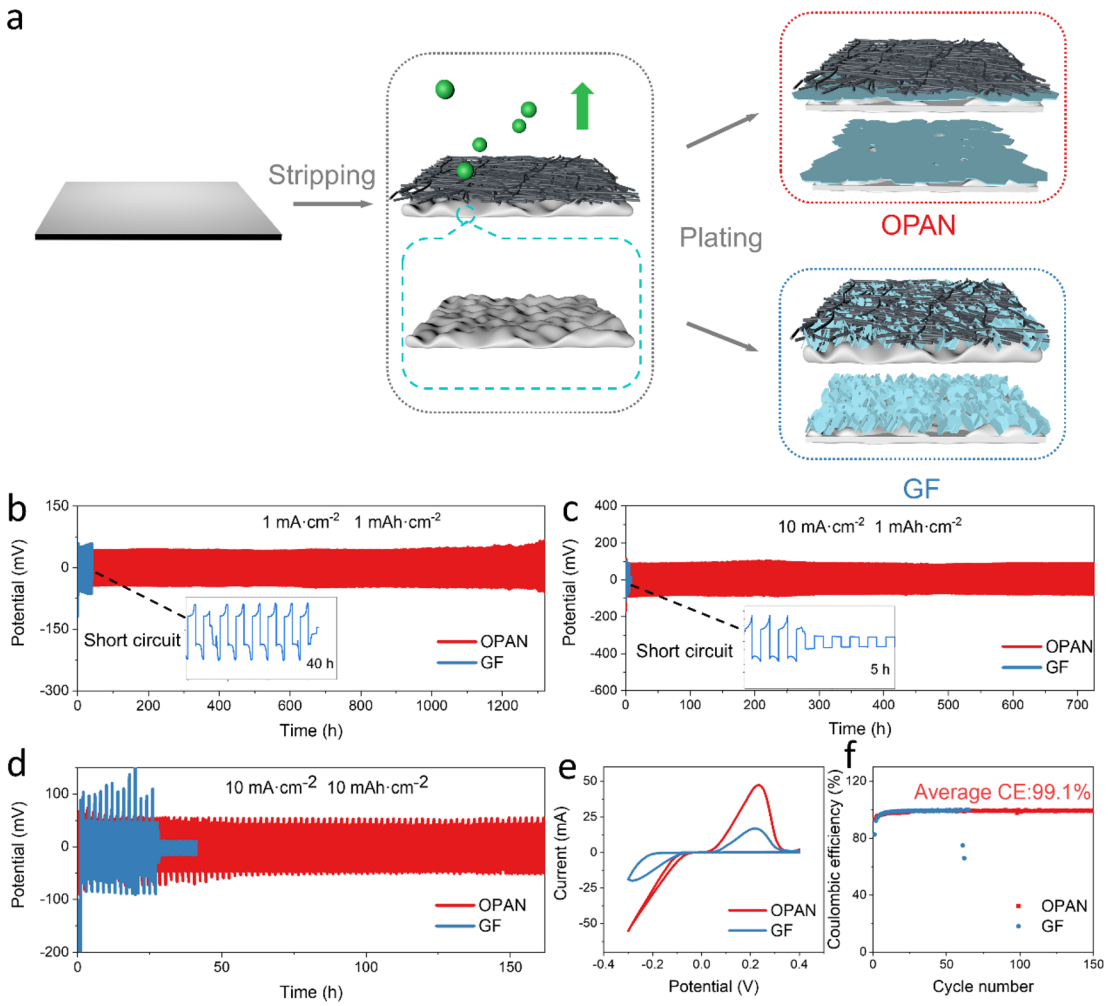

Fig. 5 (a) Schematic illustration of Zn stripping and plating with OPAN and GF separators; cycling stability of Zn symmetric batteries with OPAN and GF separators (b) at 1 mA cm^{-2} and 1 mA h cm^{-2}; (c) at 10 mA cm^{-2} and 1 mA h cm^{-2}; (d) at 10 mA cm^{-2} and 10 mA h cm^{-2}; (e) CV curves of Cu/OPAN/Zn and Cu/GF/Zn cells at 5 mV s^{-1}; (f) coulombic efficiency of Cu//Zn cells with GF and OPAN separators.

with PAN separator is also extremely unstable within these 6 hours. The large areal capacity means larger depth of discharge (DOD), which is an essential parameter to increase the actual energy density and cycle performance of a Zn metal anode.[60,61] A deeper depth (≥40% DOD_{Zn}) is required for ZIBs to reach a specific energy level that is competitive with ordinary lithium-ion batteries at the single-battery level.[14] To reveal the DOD capability of the cell using OPAN separator, we increase the areal capacity to 10 mA h cm^{-2}, equivalent to a DOD about 65% (13.79 mg Zn participating in deposition, 21.00 mg Zn overall). The symmetrical cell using OPAN separator showed a much longer lifetime of 162 h, compared with 27 h using GF separator in Fig. 5d and very unstable using PAN separator in Fig. S12d,† indicating that OPAN has good potential to reach high specific energy capacity in full cell. When the OPAN separator was taken from the cell, no significant change was observed in SEM image (Fig. S14a†), except some small crystals probably from remains of electrolyte. On the contrary, silver-gray Zn metal penetrating through the GF separator can be seen. In addition, large bulk Zn growing together with glass fibers can also be observed, which is in sharp contrast to the original GF membrane (Fig. S14b and S15†). PAN separators exhibit the same Zn dendrite piercing as GF separator, and it can be seen from SEM image (Fig. S14c†) that dendrites are tightly combined with PAN fibers.

CV curves were measured to further investigate the Zn stripping/plating behavior with OPAN and GF separators, as illustrated in Fig. 5e. In comparison to the Cu/GF/Zn cell, the Cu/OPAN/Zn cell demonstrated lower Zn plating/stripping overpotential and higher redox current density, implying improved Zn plating/stripping reversibility. The effect of the separator on the reversibility and stability of the metal Zn anode was also evaluated by using Cu//Zn asymmetrical cells at a constant areal capacity of 2 mA h cm^{-2}. As shown in Fig. 5f, the Cu/OPAN/Zn cell (93.2%) has higher initial coulombic efficiency than the Cu/GF/Zn cell (82.7%). In the subsequent cycles, the coulombic efficiency of the Cu/OPAN/Zn cells quickly rose to 99.1% in 20 cycles and remains unchanged thereafter. In contrast, the Cu/GF/Zn cell rapidly failed after only 62 cycles (Fig. 5f). In the voltage–capacity curves, the cells with OPAN separator also appeared more stable than the cell with GF

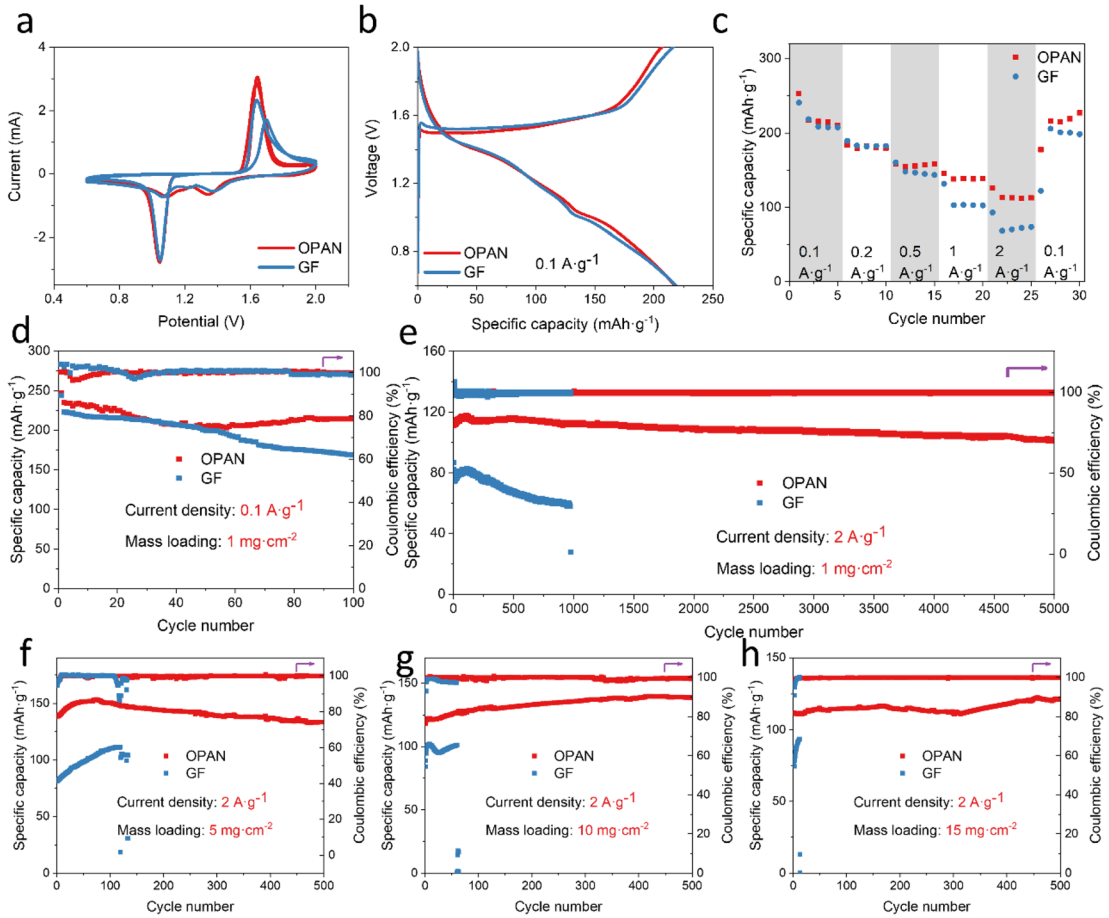

Fig. 6 Electrochemical performance of the MnO_2–Zn battery using OPAN separator and GF separator. (a) CV profiles (at 1.0 mV s^{-1}); (b) the charge/discharge curves (at 0.1 A g^{-1}); (c) rate capability plot; cycle performance at (d) 0.1 A g^{-1}, 1 mg cm^{-2}; (e) 2 A g^{-1}, 1 mg cm^{-2}; (f) 2 A g^{-1}, 5 mg cm^{-2}; (g) 2 A g^{-1}, 10 mg cm^{-2}; (h) 2 A g^{-1}, 15 mg cm^{-2} of MnO_2/OPAN/Zn and MnO_2/GF/Zn batteries.

separator. The former had almost coincided curves at the 50th and 150th cycle (Fig. S16a†), while the curves for the later one decreased significantly due to low coulombic efficiency and quick cell failure (Fig. S16b†). This might be attributed to the accumulation of uneven Zn deposits, the generation of unfavorable dendrites, and damaging side reactions.[62] After 150 cycles, XRD measurements of the Cu electrode are shown in Fig. S17.† The results confirm increased Zn (002) plane with OPAN separator. The nucleation overpotentials determined from discharge curves was lower for OPAN separator (29 mV), than the GF separator (36 mV), indicating that OPAN separator can promote the coating uniformity (Fig. S18†).

To reveal the performance of OPAN separator in full cells, MnO_2//Zn full cells with OPAN and GF separator were assembled and tested. A commercial MnO_2 was used as cathode, with its XRD (Fig. S19†) showing the pyrolusite phase MnO_2 (β-MnO_2). SEM images (the insertion of Fig. S19†) revealed that it is a heterogeneous bulk solid with diameters ranging from 1 to 15 μm. The redox reaction and reversibility during charging and discharging were studied by CV tests. CV curves of full cells using OPAN and GF separator had similar shapes and peak locations, indicating that OPAN did not alter the electrochemical process (Fig. 6a). Reversible insertion/extraction process of H^+ and Zn^{2+} into MnO_2 is represented by two groups of redox peaks.[63] Compared to MnO_2/GF/Zn batteries, MnO_2/OPAN/Zn batteries had a higher peak current density and a smaller voltage gap, indicating higher electrochemical activity and lower polarization.[64] When charged/discharged at a low current density of 0.1 A g^{-1}, their charged/discharged curves (Fig. 6b) of MnO_2/GF/Zn battery and MnO_2/OPAN/Zn battery almost overlap, but the charging capacity of GF is slightly larger, indicating lower coulombic efficiency, that is, the full battery using OPAN separator had better reversibility. The rate performance of the MnO_2/GF/Zn battery and MnO_2/OPAN/Zn battery was examined at multiple current densities ranging from 0.1 to 2 A g^{-1} (Fig. 6c). The battery with the OPAN separator performed excellently in terms of rate performance, with capacities of 216, 194, 156, 139, and 113 mA h g^{-1} at 0.1, 0.2, 0.5, 1, and 2 A g^{-1}. After the current density returned back to 0.1 A g^{-1}, its capacity recovered back to 217 mA h g^{-1}. At low current densities (0.1 A g^{-1} and 0.2 A g^{-1}), there was little difference between the full battery capacity using the GF separator and that using the OPAN separator. Full cell with GF separators had smaller capacity when the current

density increases above 0.5 A g^{-1}, which are 147 mA h g^{-1} (0.5 A g^{-1}), 103 mA h g^{-1} (1 A g^{-1}), 72 mA h g^{-1} (2 A g^{-1}). The better rate performance of the cells using OPAN separator suggests that the OPAN separator is also beneficial for fast charging. At the current density of 0.1 A g^{-1}, the MnO_2/GF/Zn cell achieved a low specific capacity of 168.7 mA h g^{-1} with a retention of 75.6% after 100 cycles. On the other hand, the MnO_2/OPAN/Zn cell maintained a higher specific capacity of 214.4 mA h g^{-1} with a retention of 91.2% after 100 cycles.

The most significant effect of OPAN separator in full cells is its improvement to the cycle lifetime. The MnO_2 cell using the OPAN separator had a 90% capacity retention (113 mA h g^{-1} at 1st cycle, 102 mA h g^{-1} at 5000th cycle) after 5000 cycles at 2 A g^{-1}, and the coulombic efficiency steadily approached 100%, indicating outstanding durability and cycle stability (Fig. 6d). While the capacity of the MnO_2 cell with the GF separator gradually decreased from 82 to 58 mA h g^{-1} and had a short circuit at the 975th cycle (Fig. S20†). The separators after cycling in full battery were also recovered for analysis. As shown in Fig. S21,† the OPAN separator was almost unchanged, while the GF separator was already merged with the Zn anode with recognizable Zn dendrites by naked eyes. The SEM images of two separators confirm the difference in Zn deposition (Fig. S22†). The surface of OPAN separator was covered with hexagonal stacked Zn, with no obvious Zn dendrites while on surface of GF separator, irregular shaped Zn crystals were mixed GF fibers. The performance in full cell confirmed that the OPAN membrane can effectively promote uniform Zn deposition and restrict dendrite growth reliably, extending the lifetime to 5000 cycles at 2 A g^{-1}.

In order to consolidate the superiority of OPAN separator in large DOD, the electrochemical performance of cells with different mass loading of MnO_2 cathode (5, 10, 15 mg cm^{-2}) were studied, and the weight of Zn is about 5 mg cm^{-2} (Table S2,† Fig. 6f–h). No matter how much the cathode material loading is, the cells using OPAN separator have a higher specific capacity and longer lifetime than using GF separator. With the loading of MnO_2 is 5, 10 and 15 mg cm^{-2}, when the OPAN separators were used, their specific capacity achieved 153.28, 139.83 and 122.50 mA h g^{-1}, and when the GF separators were used, their specific capacity only achieved 111.49, 102.00 and 93.56 mA h g^{-1}. According to the loading and the specific capacity of MnO_2, the amount of Zn anode involved in the battery reaction can be calculated. With OPAN separator, the DOD of Zn reaches 21.2%, 39.9%, or 52.5%, and all cells can run stably in 500 cycles. However, in the cells using GF separator, the DOD of Zn is 15.4%, 30.0% and 40.4%, the cycling life is only 133, 60 and 12 cycles, respectively.

4 Conclusion

In conclusion, an OPAN fiber membrane was successfully used as a Zn ion battery separator. OPAN has good wettability and electrolyte absorption, so that the electrolyte can permeate evenly and effectively reduce the local current density. The lighter weight and smaller thickness help to improve the energy density of full battery. Most importantly, OPAN with conjugated planar structure regulates Zn ions to form (002) microplates parallel to the surface of the Zn anode, thus inhibiting dendrite growth. The Zn//Zn symmetrical battery with OPAN separator has a life time of 1300 h at 1 mA cm^{-2} and 1 mA h cm^{-2}. Even under the condition of high current density (10 mA cm^{-2}) and high areal capacity (10 mA h cm^{-2}), the cycling life can be prolonged to 160 h. The average coulombic efficiency of Cu//Zn asymmetric cell with OPAN separator is 99.1%, showing good Zn stripping/platting reversibility. Based on the OPAN separator, the MnO_2//Zn full cell could perform 5000 cycles with very little attenuation at the current density of 2 A g^{-1}. Our study demonstrates that the OPAN separator can effectively regulate the Zn deposition to realize a dendrite-free Zn anode in AZIBs. Our work sheds a light to achieve practical long-life AZIBs.

Conflicts of interest

There are no conflicts to declare.

Acknowledgements

This work was supported by the Macau Science and Technology Development Fund for funding (File No. FDCT-0096/2020/A2, 0013/2021/AMJ, and 0082/2022/A2), the Multi-Year research grant (MYRG2020-00283-IAPME and MYRG2022-00266-IAPME) from the Research & Development Office at University of Macau, a grant from City University of Hong Kong (Project No. 9020002) and a grant from the Green Tech Fund (No. GTF202220105).

References

1 A. Konarov, N. Voronina, J. H. Jo, Z. Bakenov, Y.-K. Sun and S.-T. Myung, Present and future perspective on electrode materials for rechargeable zinc-ion batteries, *ACS Energy Lett.*, 2018, **3**(10), 2620–2640, DOI: **10.1021/acsenergylett.8b01552**.

2 G. Fang, J. Zhou, A. Pan and S. Liang, Recent advances in aqueous zinc-ion batteries, *ACS Energy Lett.*, 2018, **3**(10), 2480–2501, DOI: **10.1021/acsenergylett.8b01426**.

3 H. Pan, Y. Shao, P. Yan, Y. Cheng, K. S. Han, Z. Nie, C. Wang, J. Yang, X. Li and P. Bhattacharya, Reversible aqueous zinc/manganese oxide energy storage from conversion reactions, *Nat. Energy*, 2016, **1**(5), 1–7, DOI: **10.1038/nenergy.2016.39**.

4 C. Yan, X. Wang, M. Cui, J. Wang, W. Kang, C. Y. Foo and P. S. Lee, Stretchable silver-zinc batteries based on embedded nanowire elastic conductors, *Adv. Energy Mater.*, 2014, **4**(5), 1301396, DOI: **10.1002/aenm.201301396**.

5 H. Kim, J. Hong, K.-Y. Park, H. Kim, S.-W. Kim and K. Kang, Aqueous rechargeable Li and Na ion batteries, *Chem. Rev.*, 2014, **114**(23), 11788–11827, DOI: **10.1021/cr500232y**.

6 Y. Zeng, D. Luan and X. W. D. Lou, Recent advances in electrode engineering strategies for aqueous Zn-based batteries, *Chem*, 2023, **9**(5), 1118–1146, DOI: **10.1016/j.chempr.2023.03.033**.

7 P. Liang, J. Yi, X. Liu, K. Wu, Z. Wang, J. Cui, Y. Liu, Y. Wang, Y. Xia and J. Zhang, Highly reversible Zn anode enabled by controllable formation of nucleation sites for Zn-based batteries, *Adv. Funct. Mater.*, 2020, **30**(13), 1908528, DOI: **10.1002/adfm.201908528**.

8 J. Zheng, Q. Zhao, T. Tang, J. Yin, C. D. Quilty, G. D. Renderos, X. Liu, Y. Deng, L. Wang and D. C. Bock, Reversible epitaxial electrodeposition of metals in battery anodes, *Science*, 2019, **366**(6465), 645–648, DOI: **10.1126/science.aax6873**.

9 Z. Zhao, J. Zhao, Z. Hu, J. Li, J. Li, Y. Zhang, C. Wang and G. Cui, Long-life and deeply rechargeable aqueous Zn anodes enabled by a multifunctional brightener-inspired interphase, *Energy Environ. Sci.*, 2019, **12**(6), 1938–1949, DOI: **10.1039/C9EE00596J**.

10 Y. Meng, M. Wang, J. Xu, K. Xu, K. Zhang, Z. Xie, Z. Zhu, W. Wang, P. Gao and X. Li, Balancing Interfacial Reactions through Regulating p-Band Centers by an Indium Tin Oxide Protective Layer for Stable Zn Metal Anodes, *Angew. Chem.*, 2023, e202308454, DOI: **10.1002/ange.202308454**.

11 Q. Zhang, J. Luan, L. Fu, S. Wu, Y. Tang, X. Ji and H. Wang, The three-dimensional dendrite-free zinc anode on a copper mesh with a zinc-oriented polyacrylamide electrolyte additive, *Angew. Chem.*, 2019, **131**(44), 15988–15994, DOI: **10.1002/anie.201907830**.

12 Y. Zeng, X. Zhang, R. Qin, X. Liu, P. Fang, D. Zheng, Y. Tong and X. Lu, Dendrite-free zinc deposition induced by multifunctional CNT frameworks for stable flexible Zn-ion batteries, *Adv. Mater.*, 2019, **31**(36), 1903675, DOI: **10.1002/adma.201903675**.

13 B. R. Sutherland, Charging up stationary energy storage, *Joule*, 2019, **3**(1), 1–3, DOI: **10.1016/j.joule.2018.12.022**.

14 J. F. Parker, C. N. Chervin, I. R. Pala, M. Machler, M. F. Burz, J. W. Long and D. R. Rolison, Rechargeable nickel–3D zinc batteries: An energy-dense, safer alternative to lithium-ion, *Science*, 2017, **356**(6336), 415–418, DOI: **10.1126/science.aak9991**.

15 H. Qiu, X. Du, J. Zhao, Y. Wang, J. Ju, Z. Chen, Z. Hu, D. Yan, X. Zhou and G. Cui, Zinc anode-compatible in-situ solid electrolyte interphase via cation solvation modulation, *Nat. Commun.*, 2019, **10**(1), 1–12, DOI: **10.1038/s41467-019-13436-3**.

16 F. Wang, O. Borodin, T. Gao, X. Fan, W. Sun, F. Han, A. Faraone, J. A. Dura, K. Xu and C. Wang, Highly reversible zinc metal anode for aqueous batteries, *Nat. Mater.*, 2018, **17**(6), 543–549, DOI: **10.1038/s41563-018-0063-z**.

17 F. Wan, L. Zhang, X. Dai, X. Wang, Z. Niu and J. Chen, Aqueous rechargeable zinc/sodium vanadate batteries with enhanced performance from simultaneous insertion of dual carriers, *Nat. Commun.*, 2018, **9**(1), 1–11, DOI: **10.1038/s41467-018-04060-8**.

18 D. Yuan, J. Zhao, H. Ren, Y. Chen, R. Chua, E. T. J. Jie, Y. Cai, E. Edison, W. Manalastas Jr and M. W. Wong, Anion texturing towards dendrite-free Zn anode for aqueous rechargeable batteries, *Angew. Chem.*, 2021, **133**(13), 7289–7295, DOI: **10.1002/ange.202015488**.

19 K. E. Sun, T. K. Hoang, T. N. L. Doan, Y. Yu, X. Zhu, Y. Tian and P. Chen, Suppression of dendrite formation and corrosion on zinc anode of secondary aqueous batteries, *ACS Appl. Mater. Interfaces*, 2017, **9**(11), 9681–9687, DOI: **10.1021/acsami.6b16560**.

20 R. F. Ashton and M. T. Hepworth, Effect of crystal orientation on the anodic polarization and passivity of zinc, *Corrosion*, 1968, **24**(2), 50–53, DOI: **10.5006/0010-9312-24.2.50**.

21 Y. Liu, J. Hu, Q. Lu, M. Hantusch, H. Zhang, Z. Qu, H. Tang, H. Dong, O. G. Schmidt and R. Holze, Highly enhanced reversibility of a Zn anode by in-situ texturing, *Energy Storage Mater.*, 2022, **47**, 98–104, DOI: **10.1016/j.ensm.2022.01.059**.

22 Y. Yan, C. Shu, T. Zeng, X. Wen, S. Liu, D. Deng and Y. Zeng, Surface-preferred crystal plane growth enabled by underpotential deposited monolayer toward dendrite-free zinc anode, *ACS Nano*, 2022, **16**(6), 9150–9162, DOI: **10.1021/acsnano.2c01380**.

23 Y. Zeng, P. X. Sun, Z. Pei, Q. Jin, X. Zhang, L. Yu and X. W. Lou, Nitrogen-doped carbon fibers embedded with zincophilic Cu nanoboxes for stable Zn-metal anodes, *Adv. Mater.*, 2022, **34**(18), 2200342, DOI: **10.1002/adma.202200342**.

24 Y. Zeng, Z. Pei, D. Luan and X. W. D. Lou, Atomically Dispersed Zincophilic Sites in N, P-Codoped Carbon Macroporous Fibers Enable Efficient Zn Metal Anodes, *J. Am. Chem. Soc.*, 2023, **145**(22), 12333–12341, DOI: **10.1021/jacs.3c03030**.

25 H. Lu, Q. Jin, X. Jiang, Z. M. Dang, D. Zhang and Y. Jin, Vertical Crystal Plane Matching between AgZn3 (002) and Zn (002) Achieving a Dendrite-Free Zinc Anode, *Small*, 2022, **18**(16), 2200131, DOI: **10.1002/smll.202200131**.

26 Q. Li, S. Xue, P. Price, X. Sun, J. Ding, Z. Shang, Z. Fan, H. Wang, Y. Zhang and Y. Chen, Hierarchical nanotwins in single-crystal-like nickel with high strength and corrosion resistance produced via a hybrid technique, *Nanoscale*, 2020, **12**(3), 1356–1365.

27 Q. Zhang, T. Duan, M. Xiao, Y. Pei, X. Wang, C. Zhi, X. Wu, B. Long and Y. Wu, BiOI Nanopaper As a High-Capacity, Long-Life and Insertion-Type Anode for a Flexible Quasi-Solid-State Zn-Ion Battery, *ACS Appl. Mater. Interfaces*, 2022, **14**(22), 25516–25523, DOI: **10.1021/acsami.2c04946**.

28 B. Long, Q. Zhang, T. Duan, T. Song, Y. Pei, X. Wang, C. Zhi, X. Wu, Q. Zhang and Y. Wu, Few-Atomic-Layered Co-Doped BiOBr Nanosheet: Free-Standing Anode with Ultrahigh Mass Loading for "Rocking Chair" Zinc-Ion Battery, *Advanced Science*, 2022, **9**(32), 2204087, DOI: **10.1002/advs.202204087**.

29 Z. Shen, L. Luo, C. Li, J. Pu, J. Xie, L. Wang, Z. Huai, Z. Dai, Y. Yao and G. Hong, Stratified zinc-binding strategy toward prolonged cycling and flexibility of aqueous fibrous zinc metal batteries, *Adv. Energy Mater.*, 2021, **11**(16), 2100214, DOI: **10.1002/aenm.202100214**.

30 J. Ding, Z. Du, B. Li, L. Wang, S. Wang, Y. Gong and S. Yang, Unlocking the Potential of Disordered Rocksalts for Aqueous Zinc-Ion Batteries, *Adv. Mater.*, 2019, **31**(44), 1904369, DOI: **10.1002/adma.201904369**.

31 W. Zhou, M. Chen, Q. Tian, J. Chen, X. Xu and C.-P. Wong, Cotton-derived cellulose film as a dendrite-inhibiting separator to stabilize the zinc metal anode of aqueous zinc ion batteries, *Energy Storage Mater.*, 2022, **44**, 57–65, DOI: 10.1016/j.ensm.2021.10.002.

32 Y. Qin, P. Liu, Q. Zhang, Q. Wang, D. Sun, Y. Tang, Y. Ren and H. Wang, Advanced filter membrane separator for aqueous zinc-ion batteries, *Small*, 2020, **16**(39), 2003106, DOI: 10.1002/smll.202003106.

33 C. Li, Z. Sun, T. Yang, L. Yu, N. Wei, Z. Tian, J. Cai, J. Lv, Y. Shao and M. H. Rümmeli, Directly grown vertical graphene carpets as janus separators toward stabilized Zn metal anodes, *Adv. Mater.*, 2020, **32**(33), 2003425, DOI: 10.1002/adma.202003425.

34 W. Liu, S. W. Lee, D. Lin, F. Shi, S. Wang, A. D. Sendek and Y. Cui, Enhancing ionic conductivity in composite polymer electrolytes with well-aligned ceramic nanowires, *Nat. Energy*, 2017, **2**(5), 1–7, DOI: 10.1038/nenergy.2017.35.

35 W. Liu, N. Liu, J. Sun, P.-C. Hsu, Y. Li, H.-W. Lee and Y. Cui, Ionic conductivity enhancement of polymer electrolytes with ceramic nanowire fillers, *Nano Lett.*, 2015, **15**(4), 2740–2745, DOI: 10.1021/acs.nanolett.5b00600.

36 Y. Fang, X. Xie, B. Zhang, Y. Chai, B. Lu, M. Liu, J. Zhou and S. Liang, Regulating zinc deposition behaviors by the conditioner of PAN separator for zinc-ion batteries, *Adv. Funct. Mater.*, 2022, **32**(14), 2109671, DOI: 10.1002/adfm.202109671.

37 P. Chen, X. Yuan, Y. Xia, Y. Zhang, L. Fu, L. Liu, N. Yu, Q. Huang, B. Wang and X. Hu, An artificial polyacrylonitrile coating layer confining zinc dendrite growth for highly reversible aqueous zinc-based batteries, *Advanced Science*, 2021, **8**(11), 2100309, DOI: 10.1002/advs.202100309.

38 L. Sun, M. Li, L. Shang, L. Xiao, Y. Liu, M. Zhang and Y. Ao, The influence of oxygen on skin-core structure of polyacrylonitrile-based precursor fibers, *Polymer*, 2020, **197**, 122516, DOI: 10.1016/j.polymer.2020.122516.

39 J. Mittal, O. Bahl, R. Mathur and N. Sandle, IR studies of PAN fibres thermally stabilized at elevated temperatures, *Carbon*, 1994, **32**(6), 1133–1136, DOI: 10.1016/0008-6223(94)90222-4.

40 Z. Zhu, T. Jiang, M. Ali, Y. Meng, Y. Jin, Y. Cui and W. Chen, Rechargeable batteries for grid scale energy storage, *Chem. Rev.*, 2022, **122**(22), 16610–16751, DOI: 10.1021/acs.chemrev.2c00289.

41 J. Hao, X. Li, S. Zhang, F. Yang, X. Zeng, S. Zhang, G. Bo, C. Wang and Z. Guo, Designing dendrite-free zinc anodes for advanced aqueous zinc batteries, *Adv. Funct. Mater.*, 2020, **30**(30), 2001263, DOI: 10.1002/adfm.202001263.

42 Z. Luo, S. Lim, Z. Tian, J. Shang, L. Lai, B. MacDonald, C. Fu, Z. Shen, T. Yu and J. Lin, Pyridinic N doped graphene: synthesis, electronic structure, and electrocatalytic property, *J. Mater. Chem.*, 2011, **21**(22), 8038–8044, DOI: 10.1039/C1JM10845J.

43 Q. Cao, H. Gao, Y. Gao, J. Yang, C. Li, J. Pu, J. Du, J. Yang, D. Cai and Z. Pan, Regulating dendrite-free zinc deposition by 3D zincopilic nitrogen-doped vertical graphene for high-performance flexible Zn-ion batteries, *Adv. Funct. Mater.*, 2021, **31**(37), 2103922, DOI: 10.1002/adfm.202103922.

44 C. Lin, S.-H. Kim, Q. Xu, D.-H. Kim, G. Ali, S. S. Shinde, S. Yang, Y. Yang, X. Li and Z. Jiang, High-voltage asymmetric metal–air batteries based on polymeric single-Zn2+-ion conductor, *Matter*, 2021, **4**(4), 1287–1304, DOI: 10.1016/j.matt.2021.01.004.

45 D. Guo, Y. Xiao, T. Li, Q. Zhou, L. Shen, R. Li, Y. Xu and H. Lin, Fabrication of high-performance composite nanofiltration membranes for dye wastewater treatment: mussel-inspired layer-by-layer self-assembly, *J. Colloid Interface Sci.*, 2020, **560**, 273–283, DOI: 10.1016/j.jcis.2019.10.078.

46 X. Jiang, S. He, S. Li, Y. Bai and L. Shao, Penetrating chains mimicking plant root branching to build mechanically robust, ultra-stable CO 2-philic membranes for superior carbon capture, *J. Mater. Chem. A*, 2019, **7**(28), 16704–16711, DOI: 10.1039/C9TA03416A.

47 L. Shao, Z. X. Wang, Y. L. Zhang, Z. X. Jiang and Y. Y. Liu, A facile strategy to enhance PVDF ultrafiltration membrane performance via self-polymerized polydopamine followed by hydrolysis of ammonium fluotitanate, *J. Membr. Sci.*, 2014, **461**, 10–21, DOI: 10.1016/j.memsci.2014.03.006.

48 M. S. A. Rahaman, A. F. Ismail and A. Mustafa, A review of heat treatment on polyacrylonitrile fiber, *Polym. Degrad. Stab.*, 2007, **92**(8), 1421–1432, DOI: 10.1016/j.polymdegradstab.2007.03.023.

49 E. Pamula and P. G. Rouxhet, Bulk and surface chemical functionalities of type III PAN-based carbon fibres, *Carbon*, 2003, **41**(10), 1905–1915, DOI: 10.1016/S0008-6223(03)00177-5.

50 X. Qiao, C. Zhao, Z. Zhou, Q. Guan and W. Li, Constructing pyridinic N-rich aromatic ladder structure catalysts from industrially available polyacrylonitrile resin for acetylene hydrochlorination, *ACS Sustain. Chem. Eng.*, 2019, **7**(21), 17979–17989, DOI: 10.1021/acssuschemeng.9b04767.

51 T. Foroozan, V. Yurkiv, S. Sharifi-Asl, R. Rojaee, F. Mashayek and R. Shahbazian-Yassar, Non-dendritic Zn electrodeposition enabled by zincophilic graphene substrates, *ACS Appl. Mater. Interfaces*, 2019, **11**(47), 44077–44089, DOI: 10.1021/acsami.9b13174.

52 W. B. Pearson, *A handbook of lattice spacings and structures of metals and alloys: international series of monographs on metal physics and physical metallurgy*, Elsevier, 2013, vol. 4.

53 J. Zhou, M. Xie, F. Wu, Y. Mei, Y. Hao, R. Huang, G. Wei, A. Liu, L. Li and R. Chen, Ultrathin surface coating of nitrogen-doped graphene enables stable zinc anodes for aqueous zinc-Ion batteries, *Adv. Mater.*, 2021, **33**(33), 2101649, DOI: 10.1002/adma.202101649.

54 Q. Li, Y. Wang, F. Mo, D. Wang, G. Liang, Y. Zhao, Q. Yang, Z. Huang and C. Zhi, Calendar life of Zn batteries based on Zn anode with Zn powder/current collector structure, *Adv. Energy Mater.*, 2021, **11**(14), 2003931.

55 F. Mo, Z. Chen, G. Liang, D. Wang, Y. Zhao, H. Li, B. Dong and C. Zhi, Zwitterionic sulfobetaine hydrogel electrolyte building separated positive/negative ion migration

channels for aqueous Zn-MnO2 batteries with superior rate capabilities, *Adv. Energy Mater.*, 2020, **10**(16), 2000035.

56 C. Han, W. Li, H. K. Liu, S. Dou and J. Wang, Principals and strategies for constructing a highly reversible zinc metal anode in aqueous batteries, *Nano Energy*, 2020, **74**, 104880.

57 H. Lu, X. Zhang, M. Luo, K. Cao, Y. Lu, B. B. Xu, H. Pan, K. Tao and Y. Jiang, Amino acid-induced interface charge engineering enables highly reversible Zn anode, *Adv. Funct. Mater.*, 2021, **31**(45), 2103514.

58 X. Zhang, J. Li, D. Liu, M. Liu, T. Zhou, K. Qi, L. Shi, Y. Zhu and Y. Qian, Ultra-long-life and highly reversible Zn metal anodes enabled by a desolvation and deanionization interface layer, *Energy Environ. Sci.*, 2021, **14**(5), 3120–3129.

59 L. Luo, Y. Liu, Z. Shen, Z. Wen, S. Chen and G. Hong, High-Voltage and Stable Manganese Hexacyanoferrate/Zinc Batteries Using Gel Electrolytes, *ACS Appl. Mater. Interfaces*, 2023, **15**(24), 29032–29041, DOI: **10.1021/acsami.3c00905**.

60 X. Zhang, J. Li, K. Qi, Y. Yang, D. Liu, T. Wang, S. Liang, B. Lu, Y. Zhu and J. Zhou, An Ion-Sieving Janus Separator toward Planar Electrodeposition for Deeply Rechargeable Zn-Metal Anodes, *Adv. Mater.*, 2022, **34**(38), 2205175, DOI: **10.1002/adma.202205175**.

61 X. Zheng, Z. Liu, J. Sun, R. Luo, K. Xu, M. Si, J. Kang, Y. Yuan, S. Liu and T. Ahmad, Constructing robust heterostructured interface for anode-free zinc batteries with ultrahigh capacities, *Nat. Commun.*, 2023, **14**(1), 76, DOI: **10.1038/s41467-022-35630-6**.

62 Y. Jin, K. S. Han, Y. Shao, M. L. Sushko, J. Xiao, H. Pan and J. Liu, Stabilizing zinc anode reactions by polyethylene oxide polymer in mild aqueous electrolytes, *Adv. Funct. Mater.*, 2020, **30**(43), 2003932, DOI: **10.1002/adfm.202003932**.

63 M. Liu, Q. Zhao, H. Liu, J. Yang, X. Chen, L. Yang, Y. Cui, W. Huang, W. Zhao and A. Song, Tuning phase evolution of β-MnO2 during microwave hydrothermal synthesis for high-performance aqueous Zn ion battery, *Nano Energy*, 2019, **64**, 103942, DOI: **10.1016/j.nanoen.2019.103942**.

64 H. Yu, Y. Chen, H. Wang, X. Ni, W. Wei, X. Ji and L. Chen, Engineering multi-functionalized molecular skeleton layer for dendrite-free and durable zinc batteries, *Nano Energy*, 2022, **99**, 107426, DOI: **10.1016/j.nanoen.2022.107426**.